❏   1051

A modified circulating current suppression control based on MMC grid connected using NLM

H. A. Hasan[1], Riyadh Kamil Chillab[2], Ahmed K. Hannan[1], Abdelrahman Farghly[3]

[1]Council Affairs, University of Baghdad, Baghdad, Iraq
[2]Department of Electrical Engineering, College of Engineering, University of Baghdad, Baghdad, Iraq
[3]Department of Electrical Engineering, College of Engineering, University of Alexandria, Alexandria, Egypt

Article Info

ABSTRACT

High total harmonic distortion (THD) occurs when conventional circulating current suppression and modulation strategies fail to control arm circulating current in a modular multilevel converter (MMC) controlled by a virtual synchronous generator. This paper proposed a joint circulating current suppression technique that improves the proportional resonant controller's control mode and introduces the nearest level approach modulation (NLM) strategy for arm circulating current rectification. The MATLAB/Simulink program is used to conduct the simulations. The results show that: when the grid frequency does not fluctuate, the joint suppression strategy's arm current THD is 2.79%, 0.92% lower than the quasi-proportional resonant controller's (QPRC) THD; under primary frequency modulation, the suggested strategy's THD of the a-phase current is 1.75%, 1.03% lower than the QPRC's THD. Under typical operating conditions and with primary frequency management of the grid-type MMC, the results show that the proposed combined circulating current suppression technique may successfully lower total harmonic distortion (THD), eliminate bridge arm circulating current, and improve power quality.

Corresponding Author:

Ahmed K. Hannan
Council Affairs, University of Baghdad
Baghdad, Iraq
Email: ahmed.k@uobaghdad.edu.iq

1. INTRODUCTION

Renewable energy sources, such as solar and wind power, are receiving a lot of attention as a possible solution to environmental problems and global warming [1]-[3]. Several power electronic devices are needed to keep the electrical grid running steadily because renewable energy sources' power generation varies. One such device that is widely used in new technologies, such as flexible DC transmission, is the inverter, which is an essential power electronic component. Enhanced flexibility, higher conversion efficiency, and fewer losses are offered by multilevel converters, which are coupled in series with numerous submodule units, as opposed to typical converters [4]. Researchers often zero in on the modular multilevel converter (MMC) because it outperforms conventional converters in terms of stability, modularity, to achieve any voltage, scalability, low harmonics, redundancy, power-level requirements, high efficiency, high-quality waveform of voltage and current, not filter requirements [5]-[13].

With the high proportion of new energy and energy storage connected to the power system, the power system presents a "double-high form" [14], [15]. The grid-type converter using virtual synchronous generator (VSG) can provide inertia and damping for the power grid, becoming one of the effective control methods for the interaction of "grid, load, and storage" [16].

VSG-modular multilevel converter (MMC) inverter has advantages such as modularity, easy cascading, inertia, and damping, but its disadvantages are capacitor voltage fluctuation and imbalance, which causes bridge arm current waveform distortion [17], [18]. Xiong *et al.* [19] divide the circulating current method into indirect suppression and direct suppression methods. For the indirect suppression method, the circulating current is suppressed by changing the modulation wave output method. Hagiwara *et al.* [20] propose to increase the bridge arm reactance to suppress the circulating current, but it will affect the stability of the system and cannot completely eliminate the circulating current. Bruno *et al.* [21] and Yang *et al.* [22] use a parallel proportional resonant (PR) controller or a quasi-proportional resonant (QPR) controller, which can effectively suppress even harmonics, but the controller implementation is relatively complex. The literature [23], [24] uses the coordinate transformation method to convert harmonics into third harmonics, but the QPR controller has a low gain at a specific frequency, and the harmonic suppression effect is poor. For the direct suppression method, Asapu and Vanitha [25] use a current hysteresis controller to correct the nearest level approximation (NLM) modulation wave, but do not consider the influence of submodule voltage balance and the circulating current controller on the correction value.

This paper considers the infinite gain feature of the PR controller at a specific frequency, converts the negative sequence 2 times frequency circulating current and the positive sequence 4 times frequency circulating current into the third frequency circulating current, and then adopts the reduced order resonant controller (ROR) to suppress harmonics. Considering the primary frequency modulation characteristics of the VSG-MMC, a passive infrared (PIR) controller is connected in parallel to ensure harmonic suppression during frequency offset. At the same time, the suppressed harmonics are introduced into the hysteresis controller to correct the NLM modulation wave. Through the combined control strategy of direct and indirect suppression of the circulating current, the purpose of suppressing the circulating current is achieved.

2. THE OPERATING PRINCIPLE OF THE NETWORK-BASED MMC
2.1. The basic structure of MMC
The circuit structure of MMC is shown in Figure 1. Each phase has two bridge arms, upper and lower [26]. The bridge arm is composed of several sub-modules with the same structure and bridge arm inductors. By controlling the switching of sub-modules, multi-level can be achieved [27]. In Figure 1, V_{dc} is the DC bus voltage, subscripts p and n are the upper and lower bridge arms, subscript j is any one of the three phases (a,b,c), R_O and L_O are the bridge arm resistance and inductance, L_{sj} is the grid-side reactance, and V_{sj} is the grid-side voltage.
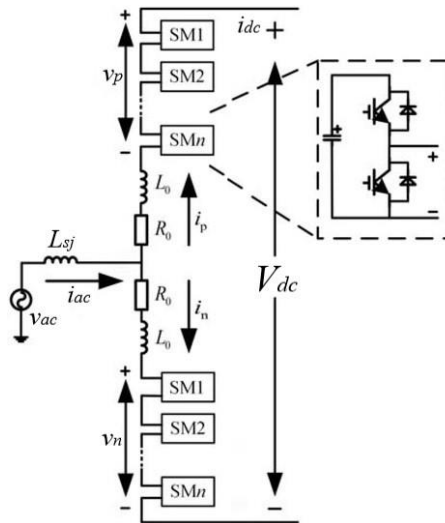

Figure 1. MMC topology [28]

2.2. Control structure of VSG-MMC
VSG control is shown in Figure 2. It mainly includes three parts: active frequency control, reactive voltage control and virtual impedance control. It can provide damping and inertia for the system [29]. Because its virtual rotor has inertia, there is an inertia in (1).

$$\begin{cases} J\frac{d\omega}{dt} = \frac{P_m}{\omega} - \frac{P_e}{\omega} - D(\omega - \omega_0) \\ P_m = P_{ref} - K_p(\omega - \omega_0) \end{cases} \tag{1}$$

In the formula, J is virtual inertia, P_m is virtual mechanical power, P_e is electromagnetic power, ω is the output angular frequency, ω_0 is rated as angular frequency, D is the damping coefficient, P_{ref} is active given value, and K_p is the active-frequency droop coefficient. The reactive droop characteristic equation is shown in (2).

$$E = E_0 + \frac{1}{s}\left[K_{q1}(V_{ref} - V_0) + K_{q2}(Q_{ref} - Q)\right] \tag{2}$$

In (2), E is the output phase voltage of VSG; V_{ref} is the phase voltage given value; V_0 is the grid-connected point voltage; Q_{ref} is the reactive power given value; K_{q1}, K_{q2} are reactive power droop coefficients. The virtual impedance control state equation is [30], [31].

$$\begin{cases} \frac{di_{vd}}{dt} = \frac{1}{L_f}\left(E_d - V_{sd} + \omega_0 L_f i_{vq} - R_f i_{vd}\right) \\ \frac{di_{vq}}{dt} = \frac{1}{L_f}\left(E_q - V_{sq} - \omega_0 L_f i_{vd} - R_f i_{vq}\right) \end{cases} \tag{3}$$

Where L_f and R_f are virtual impedances, and v is a variable inside the virtual impedance.

Figure 2. VSG control block diagram

2.3. Circulating current analysis

As shown in Figure 1, the load current i_{oj} of any phase of the MMC is evenly divided in the upper and lower bridge arms, and the influence of the circulating current i_c is considered:

$$\begin{cases} i_{pj} = i_c + \frac{i_{oj}}{2} \\ i_{nj} = i_c - \frac{i_{oj}}{2} \end{cases} \tag{4}$$

According to KVL on the bridge arm:

$$\begin{cases} -V_{dc}/2 + V_{pj} + L_0 di_{pj}/dt + R_0 i_{pj} + V_{sj} = 0 \\ -V_{dc}/2 + V_{nj} + L_0 di_{nj}/dt + R_0 i_{nj} - V_{sj} = 0 \end{cases} \tag{5}$$

Combining in (4) and in (5), we can get:

$$\begin{cases} \frac{V_{dc}}{2} - \frac{V_{pj}+V_{nj}}{2} = L_0\frac{di_{cirj}}{dt} + R_0 i_{cirj} \\ V_{cirj} = L_0\frac{di_{cirj}}{dt} + R_0 i_{cirj} \end{cases} \tag{6}$$

Through (6) and the expressions of V_a, i_a, the expression of phase circulation of phase a is derived.

$$i_{ca} = \frac{i_{dc}}{3} + I_{2f}\, sin(\omega_o\, t + \theta) \tag{7}$$

Where I_{2f} is the amplitude of the double frequency component of the circulating current. The literature [32] points out that the double frequency circulating current will cause the SM capacitor voltage to fluctuate at a triple frequency, and then generate a quadruple frequency harmonic. By analogy, the MMC circulating current only contains even harmonic components. Therefore, the corrected a phase circulating current is (8).

$$i_{ca} = \frac{i_{dc}}{3} + \sum_{m=2,4,6,\dots} I_{cirm} cos(m\omega_o + \theta) \tag{8}$$

3. PROPOSED JOINT CIRCULATION SUPPRESSION STRATEGY
3.1. Circulation extraction and transformation

From the above analysis, the AC component causes the bridge arm current distortion, and the main components are 2nd and 4th harmonics. The 2nd and 4th AC components in the circulating current are extracted using a low-pass filter. The traditional suppression method requires 4 controllers for the 2nd and 4th AC components, which increases the control difficulty. Therefore, the coordinate transformation is performed on the negative sequence 2nd frequency component and the positive sequence 4th frequency component. In the positive sequence synchronous rotating coordinate system, it can be regarded as a single-phase 3rd harmonic; that is, 2 controllers can be used for circulating current suppression. The coordinate transformation formula is (9).

$$\boldsymbol{T}_{abc/dq} = \frac{2}{3}\begin{pmatrix} \cos\theta & \cos\left(\theta - \frac{2\pi}{3}\right) & \cos\left(\theta + \frac{2\pi}{3}\right) \\ -\sin\theta & \sin\left(\theta - \frac{2\pi}{3}\right) & \sin\left(\theta + \frac{2\pi}{3}\right) \end{pmatrix} \tag{9}$$

3.2. Circulation suppressor design

The control block diagram of the resonant observer-based resonant–proportional-integral-resonant (ROR-PIR) controller is shown in Figure 3. The PR controller has a large gain attenuation outside the resonance point, but has an infinite gain at the resonance frequency. Its transfer function is:

$$G_{PR}(s) = \omega_0 s/(s^2 + \omega_0^2) \tag{10}$$

There are two conjugate resonant poles, so only the required resonant poles are retained, and the PR controller is reduced to obtain the ROR controller.

$$G_{ROR}(s) = 1/(1 - j\,\omega_0) \tag{11}$$

The ROR controller has a narrow bandwidth problem and cannot meet the suppression requirements when dealing with a frequency modulation condition. Therefore, a quasi-proportional integral resonant controller is connected in parallel on the basis of the ROR controller to meet the circulating current suppression requirements when the system frequency is offset. The transfer function of the ROR-PIR controller is:

$$\begin{cases} G_{ROR-PIR}(s) = G_{ROR}(s) + G_{PIR}(s) \\ G_{PIR}(s) = K_p + \frac{K_i}{s} + \frac{2K_r\omega_c s}{s^2 + 2\omega_c s + \omega_0^2} \end{cases} \tag{12}$$

In the formula, K_p is the proportional coefficient, K_i is the integral coefficient, K_r is the resonance coefficient, and ω_c is the cutoff frequency.

The Bode diagram of the ROR-PIR transfer function is shown in Figure 4. The resonant frequency ω_0 is 300π rad/s, and ω_c is 5π rad/s. The larger the K_r is the greater the system resonance suppression strength is. However, if K_r is too large, the system stability is relatively small. Considering the circulating current suppression strength and system stability, selecting K_r as 300 can better balance them. The dynamic response of the combined circulating current suppressor method can be slower because it relies on multiple control loops that need to coordinate and settle. The interaction between these loops can lead to a slower convergence to the steady state, especially if the system is subject to varying loads or disturbances.
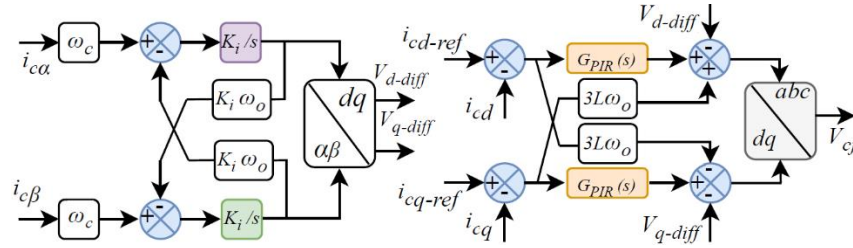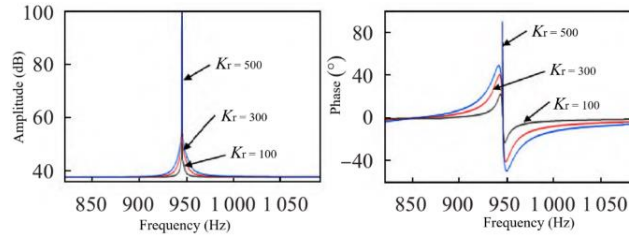
Figure 3. Circulation suppressor control block diagram

Figure 4. Bode plot of transfer function

3.3. Improved NLM

The [33]-[36] gives the number of switching of upper and lower submodules when using traditional NLM as:

$$\begin{cases} n_{pj} = \dfrac{N}{2} + round\left(\dfrac{V_{sj-ref}}{V_c}\right) \\ n_{pj} = \dfrac{N}{2} - round\left(\dfrac{V_{j-ref}}{V_c}\right) \end{cases} \tag{13}$$

where N is the number of submodules, V_{sj-ref} is the phase voltage reference value, and V_c is the initial voltage of the submodule capacitor. Ideally, the MMC outputs a phase voltage modulation value, so there is a current error $i_{diff\ j}$:

$$i_{diff\ j} + 2i_{cj} = \frac{1}{0.5L_{Oj}+L_{Sj}} \int (V_{sj-ref} - V_{sj})\, dt \tag{14}$$

Substituting (14) into (13) yields:

$$i_{diff\ j} = \frac{1}{L} \int \left(V_{sj-ref} - round\left(\frac{V_{sj-ref}+\Delta v_c}{V_c}\right) V_c\right) dt \tag{15}$$

where Δv_c is the correction value of the reference voltage output by the circulating current suppressor. According to the current error calculated by (15), the current hysteresis correction controller is designed. Figure 5 shows the current error correction waveform of the improved NLM proposed in this paper.
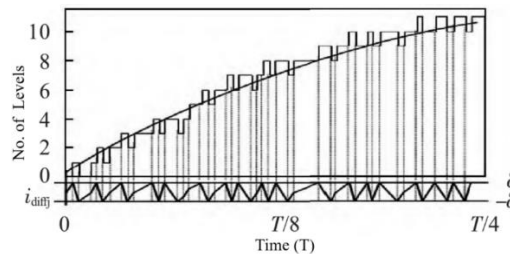
Figure 5. Improved NLM current error correction waveform

When the current error is greater than δ, the controller outputs a correction value $\Delta v = 0.5$, and when the current error is less than δ, the controller outputs a correction value $\Delta v = -0.5$. The correction value output

by the controller enters the NLM to generate an output voltage waveform. If $i_{diff\ j}$ is just at the bottom of the hysteresis loop at the current sampling moment, that is, when $i_{diff\ j} = -\delta$, the modulation output is increased by one level. Similarly, when $i_{diff\ j} = \delta$, the output is lowered by one level.

4. SIMULATION RESULTS ANALYSIS AND DISCUSSION

In order to verify the effectiveness of the joint circulation suppression strategy proposed in this paper, a 23-level VSG-MMC with 22 submodule per arm, the submodule capacitance 7000 µF with 500 V ($\frac{V_{dc}}{N}$) was built in MATLAB/Simulink environment. The simulation model as shown in Figure 6, and the system parameters are shown in Table 1.

Table 1. System parameters

Parameter	Value	Parameter	Value
DC link voltage V_{dc}	11 kV	Resonance gain K_r	300
AC side voltage	6.6 kV	Cutoff frequency ω_r	5
Frequency	50 Hz	Resonance frequency ω_o	$300\,\pi$
Bridge arm inductance	13.5 µH	Grid side inductance L_s	13.85 µH
Bridge arm resistance	1 Ω	Moment of inertia J	3.5/(kg·m²)
Proportional coefficient K_p	50	Damping coefficient	350
Integration coefficient K_i	100		
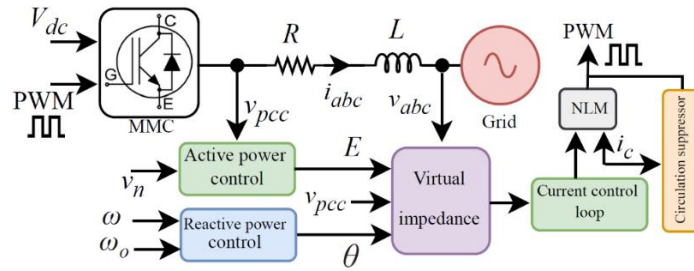
Figure 6. VSG-MMC control structure

4.1. Primary frequency modulation condition

The grid-side frequency is set to 49.8 Hz, the circulating current suppressor is put into operation at 0.5 s, and the grid-side frequency is reduced by 0.2 Hz, which takes effect when the simulation time is 1.5 to 2.5 s. The simulation results are as:

4.1.1. Comparison between QPR controller and the controller proposed in this paper:

The output current waveform and circulating current waveform of the QPR AC side is shown in Figure 7(a). Before the circulating current suppressor is turned on at 0.5s, its total harmonic distortion rate (THD) is 3.26%; after the circulating current suppressor is turned on, before the first frequency modulation is started, THD is 2.82%; during the first frequency modulation, the base frequency is 49.8 Hz, and its THD value is 2.78%. When the QPR controller responds to the frequency fluctuation on the grid side, its circulating current fluctuation value is about 5 A. Compared with the combined circulating current suppressor in Figure 7(b), its advantage is that the current fluctuation before and after the circulating current suppressor is turned on is small.

The circulating current combined suppressor proposed in this paper has a THD of 3.38% before the circulating current suppressor is turned on at 0.5s; after the circulating current suppressor is turned on, the THD before the first frequency modulation is started is 2.59%; during the first frequency modulation, the THD value is 1.75%. When the combined circulating current suppressor responds to the grid-side frequency fluctuation, the fluctuation value is about 3.5 A. Therefore, the circulating current combined suppressor proposed in this paper is more suitable for the working conditions of grid frequency fluctuation.

4.1.2. Primary frequency modulation, power, and voltage response:

Figure 8(a) shows the result of the system frequency dynamic response. When the circulating current suppressor is connected to the system and the grid-side frequency changes, oscillation occurs. The reason is that the VSG system is difficult to take into account the grid-connected active power dynamic characteristics and droop characteristics. This paper combines the droop characteristics and damping characteristics to make the

oscillation range within 0.05 Hz. Figure 8(b) is the system power dynamic response waveform. Its grid-connected active power oscillates; the reactive power starts to increase when the system frequency decreases, maintaining the grid-connected voltage amplitude without fluctuations. At the same time, the system has damping and inertia.
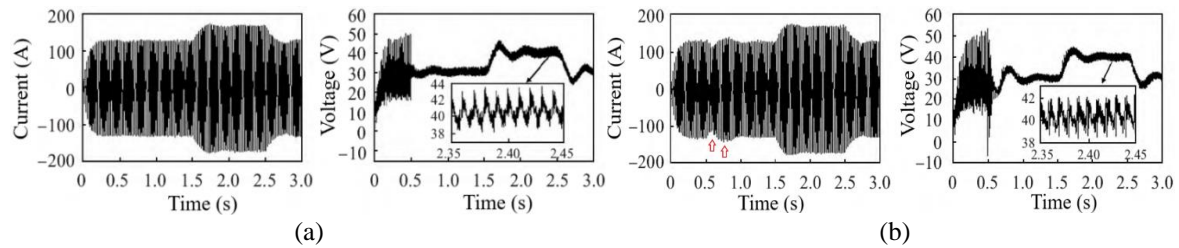

(a)   (b)

Figure 7. Output current waveform and circulating current waveform of phase an AC side when the grid frequency fluctuates (a) QPR circulating current suppressor and (b) combined circulating current suppressor

(a)   (b)
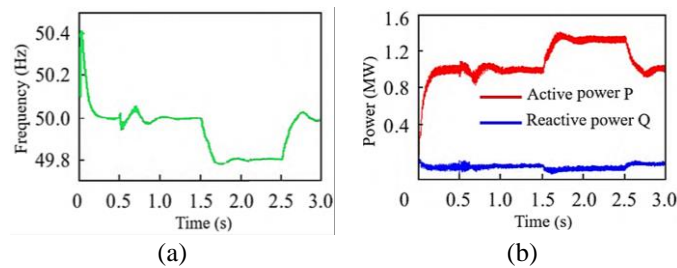
Figure 8. System dynamic response: (a) system frequency dynamic response and (b) system power response

4.2. Steady state

Figure 9 shows the waveform of the circulating current on the bridge arm on phase a and the FFT analysis diagram. The circulating current suppressors are all put into operation at 0.5s. Figure 9(a) is the waveform of the circulating current without the circulating current suppressor. The fluctuation range of the circulating current after stabilization is about 15-55 A. The waveform distortion of the bridge arm current is mainly affected by the harmonic components of the 2-fold and 4-fold frequency circulating current. Figure 9(b) is the waveform of the circulating current with the QPR circulating current suppressor. The fluctuation range of the circulating current after steady state is about 28.5-33 A. Compared with the case without the circulating current suppressor, the fluctuation range is reduced by about 88.75%. Figure 9(c) is the circulating current combined suppression method of the ROR-PIR circulating current suppressor and the improved NLM.

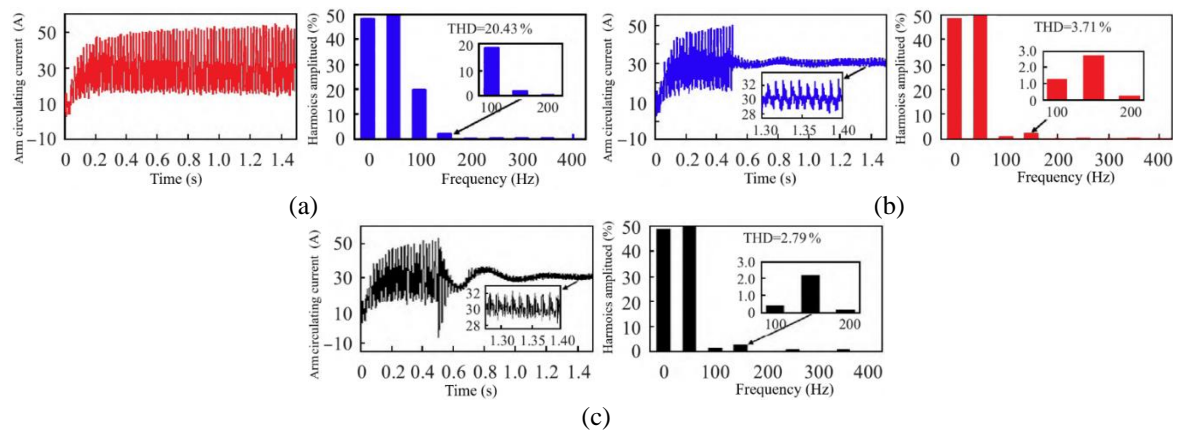(a)   (b)

(c)

Figure 9. Phase an upper arm circulating current waveform and FFT analysis: (a) circulating current without the circulating current suppressor, (b) QPR circulating current suppressor, and (c) combined circulating current suppressor

At 0.5 s, the circulating current is stabilized by 1.5-2.5 A. After the circulating current suppressor is put into use, the system reaches stability about 0.2s slower than the QPR circulating current suppression method due to its more complex control structure, the need for coordination between multiple control loops, and the potential for slower dynamic response, but after reaching stability, the circulating current fluctuation range is about 29-32A, and the fluctuation range is reduced by about 92.5% compared with no circulating current suppressor. It can be seen that: the proposed circulating current suppression method has better suppression effects on the 2-fold and 4-fold frequency components than the QPR controller, and for the 3-fold frequency component, the improved NLM modulation strategy optimizes the submodule capacitor voltage, making its 3-fold frequency fluctuation less, so the proposed circulating current suppression strategy is better than the effect of the QPR circulating current suppressor.

5. CONCLUSION

In this paper, the proportional resonant controller's control mode is improved, and the nearest level approach modulation (NLM) strategy for arm circulating current rectification is introduced. The simulation results show that: i) When the system is stable, the proposed joint suppression strategy for the circulating current has infinite gain at a specific frequency due to the ROR controller; ii) The parallel connection of the PIRR controller gives the proposed strategy a higher bandwidth when the system frequency fluctuates, suppressing the frequency shifts and avoiding the PR controller's narrow bandwidth. The improved NLM modulation method further stabilizes the three SM voltage oscillations; and iii) When the VSG-MMC system built in this paper is connected to the grid, the droop coefficient and damping coefficient are adjusted to keep its frequency fluctuation within 0.05 Hz, the three-phase voltage waveform is unaffected by the circulating current suppressor switching and grid-side frequency fluctuation, and the system has damping and inertia.

AUTHOR CONTRIBUTIONS STATEMENT

This journal uses the Contributor Roles Taxonomy (CRediT) to recognize individual author contributions, reduce authorship disputes, and facilitate collaboration.

Name of Author	C	M	So	Va	Fo	I	R	D	O	E	Vi	Su	P	Fu
H. A. Hasan	✓	✓	✓	✓	✓	✓		✓	✓	✓			✓	✓
Riyadh Kamil Chillab		✓	✓			✓		✓	✓	✓	✓	✓		✓
Ahmed K. Hannan	✓		✓	✓			✓		✓		✓	✓	✓	✓
Abdelrahman Farghly		✓	✓	✓			✓	✓		✓	✓			✓

C	:	**C**onceptualization	I	:	**I**nvestigation	Vi	:	**Vi**sualization
M	:	**M**ethodology	R	:	**R**esources	Su	:	**Su**pervision
So	:	**So**ftware	D	:	**D**ata Curation	P	:	**P**roject administration
Va	:	**Va**lidation	O	:	Writing - **O**riginal Draft	Fu	:	**Fu**nding acquisition
Fo	:	**Fo**rmal analysis	E	:	Writing - Review & **E**diting			

CONFLICT OF INTEREST

The authors declare that they have no known competing financial interests or personal relationships that could have appeared to influence the work reported in this paper

DATA AVAILABILITY

The data that support the findings of this study are openly available in https://2cm.es/VDUd at DOI: https://2cm.es/VDUB.

REFERENCES

[1]   E. H. Ibrahem, N. Q. Mohammed, and H. M. D. Habbi, "Microgrid integration based on deep learning NARMA-L2 controller for maximum power point tracking," *Journal of Engineering*, vol. 29, no. 10, pp. 12–32, 2023, doi: 10.31026/j.eng.2023.10.02.

[2]   A. K. Abdullah and H. M. D.Habbi, "Enhancing sustainable energy integration with a techno-economic evaluation of hybrid renewable energy systems at the College of Engineering in the University of Baghdad," *Journal of Engineering*, vol. 30, no. 11, pp. 71–89, Nov. 2024, doi: 10.31026/j.eng.2024.11.05.

[3]   V. Sidorov, A. Bakeer, H. M. Maheri, N. Hassanpour, S. Rahman, and A. Chub, "Shade-tolerant PV micro converters," *Distributed Energy Systems*, pp. 261–282, 2022, doi: 10.1201/9781003229124-17.

[4]   S. R. Hameed and T. H. Al-Mhana, "Cascaded H–bridge multilevel inverter: Review of topologies and pulse width modulation. Tikrit Journal of Engineering Sciences," *Tikrit Journal of Engineering Sciences*, vol. 31, no. 1, pp. 138–151, 2024, doi: 10.25130/tjes.31.1.12.

[5]   J. V. M. Farias, L. A. Gregoire, A. F. Cupertino, H. A. Pereira, S. I. Seleme, and M. Fadel, "A sliding-mode observer for MMC-HVDC systems: Fault-tolerant scheme with reduced number of sensors," *IEEE Transactions on Power Delivery*, vol. 38, no. 2, pp. 867–876, 2023, doi: 10.1109/TPWRD.2022.3200419.

[6]   Z. Wang, "Recent advances in circulating current suppression strategies for modular multilevel converters," *Journal of Physics: Conference Series*, vol. 2786, no. 1, 2024, doi: 10.1088/1742-6596/2786/1/012001.

[7]   H. S. Jouybary, A. Mpanda Mabwe, D. Arab Khaburi, and A. El Hajjaji, "An LMI-based linear quadratic regulator (LQR) control for modular multilevel converters (MMCs) considering parameters uncertainty," *IEEE Access*, vol. 12, pp. 111888–111898, 2024, doi: 10.1109/ACCESS.2024.3442090.

[8]   Q. Shu and G. Chen, "Research on circulating current suppression strategy of modular multilevel converter," in *Sixth International Conference on Electromechanical Control Technology and Transportation (ICECTT 2021)*, Q. Zeng, Ed., SPIE, Feb. 2022, p. 38. doi: 10.1117/12.2623874.

[9]   M. A. Perez, S. Ceballos, G. Konstantinou, J. Pou, and R. P. Aguilera, "Modular multilevel converters: Recent achievements and challenges," *IEEE Open Journal of the Industrial Electronics Society*, vol. 2, pp. 224–239, 2021, doi: 10.1109/OJIES.2021.3060791.

[10] R. Hu, "Comprehensive analysis on topological structure of modular multilevel converters," *Highlights in Science, Engineering and Technology*, vol. 81, pp. 26–37, Jan. 2024, doi: 10.54097/gha3n157.

[11] R. Alaei and S. A. Khajehoddin, "Series hybrid modular multilevel converter for HVDC transmission systems," *IEEE Access*, vol. 12, pp. 76816–76825, 2024, doi: 10.1109/ACCESS.2024.3406739.

[12] B. Li, S. Zhou, D. Xu, S. J. Finney, and B. W. Williams, "A hybrid modular multilevel converter for medium-voltage variable-speed motor drives," *IEEE Transactions on Power Electronics*, vol. 32, no. 6, pp. 4619–4630, 2017, doi: 10.1109/TPEL.2016.2598286.

[13] M. Kurtoğlu, F. Eroğlu, A. O. Arslan, and A. M. Vural, "Recent contributions and future prospects of the modular multilevel converters: A comprehensive review," *International Transactions on Electrical Energy Systems*, vol. 29, no. 3, 2019, doi: 10.1002/etep.2763.

[14] P. Hu, Y. Li, Y. Yu, and F. Blaabjerg, "Inertia estimation of renewable-energy-dominated power system," *Renewable and Sustainable Energy Reviews*, vol. 183, 2023, doi: 10.1016/j.rser.2023.113481.

[15] H. A. Alnaieli, A. A. Jadallah, and A. H. Numan, "Design, fabrication, and experimental analysis of a PV panel for a smart sunflower system," *Tikrit Journal of Engineering Sciences*, vol. 31, no. 1, pp. 113–126, 2024, doi: 10.25130/tjes.31.1.10.

[16] A. Lunardi, L. F. N. Lourenço, E. Munkhchuluun, L. Meegahapola, and A. J. S. Filho, "Grid-connected power converters: an overview of control strategies for renewable Energy," *Energies*, vol. 15, no. 11, 2022, doi: 10.3390/en15114151.

[17] C. Li, Y. Cao, Y. Yang, L. Wang, F. Blaabjerg, and T. Dragicevic, "Impedance-based method for DC stability of VSC-HVDC system with VSG control," *International Journal of Electrical Power and Energy Systems*, vol. 130, 2021, doi: 10.1016/j.ijepes.2021.106975.

[18] M. Li *et al.*, "Phase feedforward damping control method for virtual synchronous generators," *IEEE Transactions on Power Electronics*, vol. 37, no. 8, pp. 9790–9806, 2022, doi: 10.1109/TPEL.2022.3150950.

[19] X. Xiong, X. Wang, D. Liu, F. Blaabjerg, and C. Zhao, "Common-mode insertion indices compensation with capacitor voltages feedforward to suppress circulating current of MMCS," *CPSS Transactions on Power Electronics and Applications*, vol. 5, no. 2, pp. 103–113, 2020, doi: 10.24295/CPSSTPEA.2020.00009.

[20] M. Hagiwara, R. Maeda, and H. Akagi, "Theoretical analysis and control of the modular multilevel cascade converter based on double-star chopper-cells (MMCC-DSCC)," in *2010 International Power Electronics Conference - ECCE Asia -, IPEC 2010*, 2010, pp. 2029–2036. doi: 10.1109/IPEC.2010.5543517.

[21] B. E. Bruno, I. R. F. M. P. da Silva, C. B. Jacobina, and A. C. Oliveira, "Modular multilevel cascade converters," in *Power Electronic Converters and Systems: 2nd Edition: Converters and machine drives*, 2024, pp. 119–152. doi: 10.1049/pbpo241f_ch4.

[22] S. Yang, K. Liu, L. Qin, S. Zhu, B. Xu, and Q. Wang, "A broadband active damping method for high-frequency resonance suppression in MMC-HVDC system," *International Journal of Electrical Power and Energy Systems*, vol. 146, 2023, doi: 10.1016/j.ijepes.2022.108791.

[23] G. Keiel, J. V. Flores, and L. F. A. Pereira, "On the robust control design of multiple resonant controllers for the parallel operation of UPSs," *Control Engineering Practice*, vol. 147, 2024, doi: 10.1016/j.conengprac.2024.105925.

[24] G. Fu and Z. Lu, "MMC circulating current suppression strategy based on improved quasi-PR control," *Frontiers in Computing and Intelligent Systems*, vol. 3, no. 2, pp. 16–20, 2023, doi: 10.54097/fcis.v3i2.6911.

[25] S. Asapu and R. Vanitha, "Modified hysteresis current control of multilevel converter for grid connected battery storage system," *Materials Today: Proceedings*, vol. 80, pp. 3523–3531, 2023, doi: 10.1016/j.matpr.2021.07.290.

[26] F. Martinez-Rodrigo, D. Ramirez, A. B. Rey-Boue, S. De Pablo, and L. C. Herrero-De Lucas, "Modular multilevel converters: Control and applications," *Energies*, vol. 10, no. 11, 2017, doi: 10.3390/en10111709.

[27] A. K. Hannan, Z. A. Kadhum, A. K. Ali, A. Farghly, and L. K. Hanan, "Suppression of the capacitor voltage ripple in modular multilevel converter for variable-speed drive applications," *Tikrit Journal of Engineering Sciences*, vol. 31, no. 1, pp. 56–74, 2024, doi: 10.25130/tjes.31.1.6.

[28] X. Tian, Y. Ma, J. Yu, C. Wang, and H. Cheng, "A modified one-cycle-control method for modular multilevel converters," *Energies*, vol. 12, no. 1, 2019, doi: 10.3390/en12010157.

[29] S. HosseinNataj, S. A. Gholamian, M. Rezanejad, and M. Mehrasa, "Virtual synchronous generator-based control of modular multilevel converter for integration into weak grid," *IET Renewable Power Generation*, vol. 17, no. 12, pp. 3097–3107, 2023, doi: 10.1049/rpg2.12828.

[30] W. Du, H. Wang, and L. Y. Xiao, "Power system small-signal stability as affected by grid-connected photovoltaic generation," *European Transactions on Electrical Power*, vol. 22, no. 5, pp. 688–703, 2012, doi: 10.1002/etep.598.

[31] S. Lu *et al.*, "Small-signal stability research of grid-connected virtual synchronous generators," *Energies*, vol. 15, no. 19, 2022, doi: 10.3390/en15197158.

[32] A. K. Hannan and T. K. Hassan, "Design and simulation of modular multilevel converter fed induction motor drive," *Indonesian Journal of Electrical Engineering and Informatics*, vol. 9, no. 1, pp. 22–36, 2021, doi: 10.11591/ijeei.v9i1.2699.

[33] M. Kurtoğlu and A. M. Vural, "A Novel Nearest Level Modulation Method with Increased Output Voltage Quality for Modular Multilevel Converter Topology," *International Transactions on Electrical Energy Systems*, vol. 2022, pp. 1–17, Jan. 2022, doi: 10.1155/2022/2169357.

[34] H. M. Almgotir, E. A. Khaliq Ali, W. H. Abd Al Ameer, and M. A. Fadel Al-Qaisi, "Harmonics elimination for DC/DC power supply based on piezoelectric filters," *International Journal of Power Electronics and Drive Systems*, vol. 12, no. 1, pp. 356–363, 2021, doi: 10.11591/ijpeds.v12.i1.pp356-363.

[35] S. T. Y. Alfalahi, M. Bin Mansor, H. M. Kadhim, and R. M. Alsammarraie, "Improvement of distribution substation performance using SVC and a grid-tied solar PV system," *IOP Conference Series: Earth and Environmental Science*, vol. 1440, no. 1, 2025, doi: 10.1088/1755-1315/1440/1/012002.

[36] A. Farghly, A. Elserougi, A. Abdel-khalik, and R. Hamdy, "A hybrid mixed-cells DC-DC modular multilevel converter with balanced arm energy and DC fault blocking capability for high voltage direct current systems," *International Journal of Circuit Theory and Applications*, vol. 52, no. 9, pp. 4556–4581, 2024, doi: 10.1002/cta.3944.

BIOGRAPHIES OF AUTHORS

H. A. Hasan was born in 1983. He received a B.Sc. in electrical power and machine engineering from the University of Diyala in 2005, and an M.Sc. in electrical engineering Department in Electrical Power and Machine Engineering at the University of Baghdad in 2008. Then he joined the Advanced High Voltage Engineering Center in the Electrical and Electronic Engineering Department at Cardiff University, Wales, UK, to finish his Ph.D. in 2017. He can be contacted at email: hasanha@avic.uobaghdad.edu.iq.

Riyadh Kamil Chillab received the B.S. in Electrical Engineering Department at Al-Mustansiriyah University in Iraq (2003); he is doing a Master of Electrical Engineering, Baghdad University, Iraq. He is interested in the following fields: electrical power engineering, electrical machines, and induction heating. He is currently a Lecturer at the Department of Electrical Engineering, College of Engineering, University of Baghdad, Iraq. He can be contacted at email: riyadh.k@coeng.uobaghdad.edu.iq.

Ahmed K. Hannan was born in 1993. He received a B.Sc. degree in Electrical Engineering in 2015 and a M.Sc. degree in Electrical Engineering, Power and Machines in 2020 from the Electrical Engineering Department, College of Engineering, Mustansiriyah University, Iraq. From 2015 to 2018, he was working as an electrical engineer with ABB, Erbil, Iraq. From 2020 up to now, he was an electrical engineer, council affairs, University of Baghdad. His research interests include high-frequency DC-DC converters, AC drive systems, grid-connected photovoltaic systems, high-power electronics, multilevel converters, control algorithms, microgrid, and PWM techniques. He can be contacted at email: ahmed.k@uobaghdad.edu.iq.

Abdelrahman Farghly received B.Sc. and M.Sc. degrees in electrical engineering from Alexandria University, Alexandria, Egypt, in 2014 and 2020. He is currently a Ph.D. student and lecturer assistant with the Electrical Engineering Department, Faculty of Engineering, Alexandria University, Alexandria, Egypt. His current research interests include electric drives, multiphase machines, battery chargers, renewable energy resources, and power electronics. He can be contacted at email: abdelrahman.farghly@alexu.edu.eg.